



OPEN

Breakdown of Richardson's Law in Electron Emission from Individual Self-Joule-Heated Carbon Nanotubes

SUBJECT AREAS:
ELECTRONIC PROPERTIES
AND MATERIALSCARBON NANOTUBES AND
FULLERENES

Xianlong Wei, Sheng Wang, Qing Chen & Lianmao Peng

Received
27 February 2014Accepted
9 May 2014Published
29 May 2014Correspondence and
requests for materials
should be addressed to
X.W. (weixl@pku.edu.cn)

Key Laboratory for the Physics and Chemistry of Nanodevices, Department of Electronics, Peking University, Beijing 100871, P. R. China.

Probing the validity of classical macroscopic physical laws at the nanoscale is important for nanoscience research. Herein, we report on experimental evidence that electron emission from individual hot carbon nanotubes (CNTs) heated by self-Joule-heating does not obey Richardson's law of thermionic emission. By using an *in-situ* multi-probe measurement technique, electron emission density (J) and temperature (T) of individual self-Joule-heated CNTs are simultaneously determined. Experimental $\ln(J/T^2) - 1/T$ plots are found to exhibit an upward bending feature deviating from the straight lines in Richardson plots, and the measured electron emission density is more than one order of magnitude higher than that predicted by Richardson's law. The breakdown of Richardson's law implies a much better electron emission performance of individual CNTs as compared to their macroscopic allotropes and clusters, and the need of new theoretical descriptions of electron emission from individual low-dimensional nanostructures.

Electron emission from a solid is an important phenomenon that has wide applications and has played irreplaceable roles in the progresses of electronics and physics. The laws governing the behaviors of electron emission include Richardson's law for thermionic emission and Fowler–Nordheim law for field emission. The two laws were derived on the basis of Sommerfeld free electron model^{1,2}, where the Fermi–Dirac statistics is applied to an atmosphere of three-dimensional (3D) free electrons in metals. So they were originally proposed to describe electron emission from macroscopic bulk metals. In recent years, thermionic electron emission and field electron emission from low-dimensional nanostructures, *e.g.* carbon nanotubes (CNTs), graphenes, *etc.*, have been widely studied and found to exhibit outstanding performances^{3–9}. To interpret the measured emission current from low-dimensional nanostructures, the macroscopic Richardson's law and Fowler–Nordheim law were usually directly adopted in previous reports^{3,4,6–8}. Therefore, it is important to probe the validity of the macroscopic laws at the nanoscale.

The validity of the macroscopic Richardson's law and Fowler–Nordheim law at the nanoscale is highly controversial up to date. On the one hand, since Richardson's law and Fowler–Nordheim law were derived on the basis of 3D Sommerfeld free electron model as mentioned above^{1,2}, they cannot be applied to electron emission from low-dimensional nanostructures that deviate much from 3D free electron systems. On the other hand, previous experimental results showed quite conflicting conclusions on their validity at the nanoscale. While thermionic emission from the yarns of CNTs was observed to obey Richardson's law very well^{4,10,11}, and field emission from both CNT/graphene arrays and individual CNTs was observed to follow Fowler–Nordheim law in some reports^{6–8,12,13}, field emission from CNT arrays and individual single-layer graphenes were also observed to deviate from Fowler–Nordheim law in a few other reports^{9,14}. Therefore, it is highly imperative to end the controversy through well-designed experimental measurements, where emission current density of individual low-dimensional nanostructures and emitter temperature for thermionic emission or local pulling electric field for field emission should be both accurately determined. To date, such measurements have never been achieved due to great challenges. Even though field emission from individual nanostructures were studied in several reports^{6,7,9,13}, local electric field at the sharp emitting apex of nanostructures in those reports were determined not by direct measurements, but by fitting experimental data with Fowler–Nordheim law through introducing a field enhancement factor.

Herein, by using a delicate *in-situ* multi-probe measurement technique which ingeniously combines three electrical probes and one optical probe installed in a scanning electron microscope (SEM), we succeed in simultaneously determining both the electron emission density (J) and the temperature (T) of individual hot



CNTs heated by self-Joule heating. It is found that experimental $\ln(J/T^2)-1/T$ plots exhibit an upward bending feature obviously deviating from the straight lines in Richardson plots, and that the measured electron emission density is more than one order of magnitude higher than that predicted by Richardson's law. We present conclusive experimental evidence that electron emission from individual self-Joule-heated CNTs does not obey classical macroscopic Richardson's law, indicating the breakdown of the macroscopic law of electron emission at the nanoscale.

Results

As schematically shown in Fig. 1a, an individual CNT was firstly suspended between two electrical probes through delicate nanomanipulations. After good electrical contacts between CNT and electrical probes were established (the contact resistance between CNT and electrical probes was measured to be $\sim 4.8 \text{ k}\Omega$ as shown in Supplementary Fig. S1 online), a bias voltage (V_{bias}), thus an electrical current (I_{bias}), was applied to the CNT to heat it up through self-Joule heating and induce electron emission from its side surface. The third electrical probe with a collecting voltage (V_{collect}) applied was placed close to the middle of the CNT to collect emitted electrons and emission current (I_{collect}) was measured. At the same time, thermal light emission from the CNT was collected by an optical probe and thermal emission spectra were recorded. The ingenious combination of three electrical probes and one optical probe enables us to achieve simultaneous measurements of electron emission current and thermal emission spectra from the same individual CNTs. SEM images of a CNT under measurements are shown in Fig. 1b and 1c. After measurements in SEM were completed, the CNTs were transferred to a transmission electron microscope (TEM) for

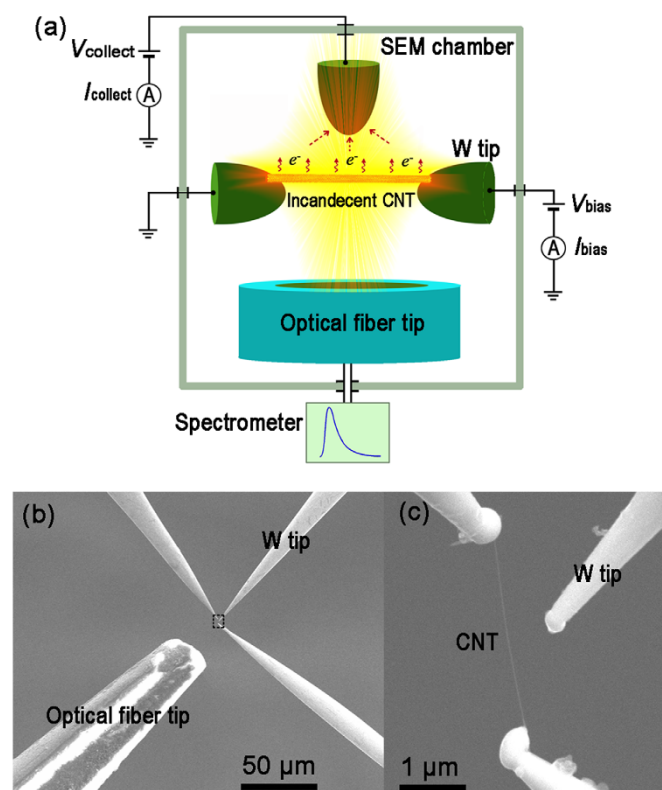


Figure 1 | Multi-probe measurement setup. (a) A schematic drawing of the experimental setup. (b) A SEM image showing the simultaneous measurements of electron emission current and thermal emission spectra from individual Joule-heated CNTs by combining three electrical probes (W tips) and one optical probe (optical fiber tip). (c) An enlarged SEM image of the framed area in (b).

diameter measurement¹⁵, which enables us to accurately determine the side surface area of a CNT and calculate emission density from measured emission current.

Figure 2 shows the results of electrical measurements on a CNT with a diameter of 17 nm and a length of 5.7 μm . The $I_{\text{bias}}-V_{\text{bias}}$ plot exhibits a typical feature for a multiwalled CNT with a saturation region at high bias voltage range (Fig. 2a)¹⁶. Emission current (I_{collect}) started to become measurable when V_{bias} located at the saturation region, namely larger than about 2.8 V for the CNT. We measured $I_{\text{collect}}-V_{\text{collect}}$ plots when V_{bias} increased from 2.87 to 3.21 V at intervals of 0.01 V and the plots with V_{bias} from 2.97 to 3.21 V at 0.04 V intervals are shown in Fig. 2b. It can be seen that, similar to thermionic emission characteristics from bulk metals, each $I_{\text{collect}}-V_{\text{collect}}$ plot exhibits a fast increasing region followed by a slow increasing one. The local electric field at the surface of a CNT corresponding to the V_{collect} we applied was calculated to be less than $\sim 10^8 \text{ V m}^{-1}$, which is much lower than that needed for field emission ($\sim 10^9 \text{ V m}^{-1}$)¹⁷. So tunneling dominated field emission is excluded here. The slow increasing region in Fig. 2b is attributed to accelerating field regime as a result of the Schottky effect and the fast

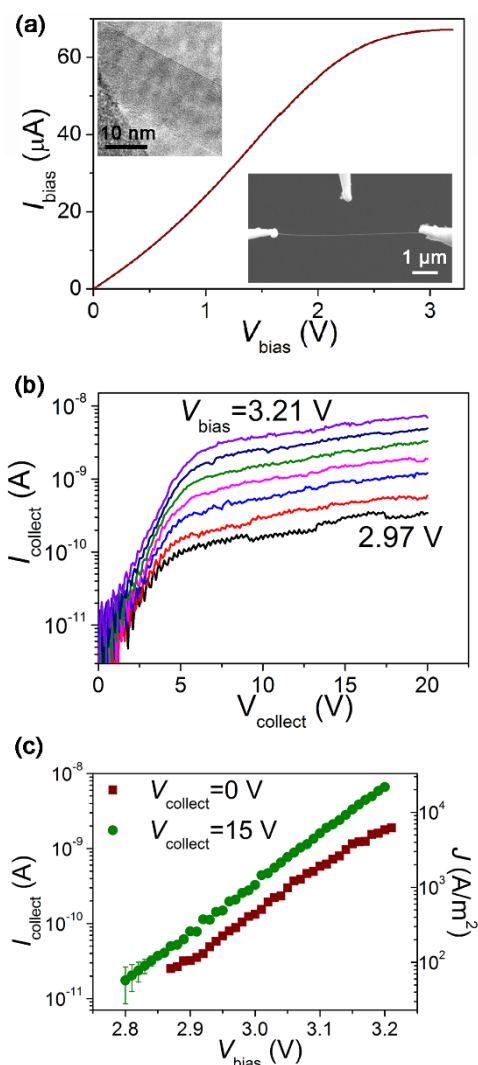


Figure 2 | Electrical measurements on a CNT. (a) $I_{\text{bias}}-V_{\text{bias}}$ plot of a CNT with a diameter of 17 nm and a length of 5.7 μm . The bottom-right inset is a SEM image of the CNT under measurement and the up-left inset is its TEM image after measurements. (b) $I_{\text{collect}}-V_{\text{collect}}$ plots of the CNT with V_{bias} ranging from 2.97 to 3.21 V at 0.04 V intervals. (c) $I_{\text{collect}}-V_{\text{bias}}$ and $J-V_{\text{bias}}$ plots of the CNT with $V_{\text{collect}} = 0$ and 15 V.



increasing one is attributed to space charge regime. In accelerating field regime, I_{collect} is observed to increase exponentially with V_{collect} , which is different from the exponential dependence of I_{collect} on $V_{\text{collect}}^{1/2}$ for the Schottky effect in bulk thermionic emitters¹⁸. The difference is attributed to the breakdown of classical image potential, which is responsible for the exponential dependence of I_{collect} on $V_{\text{collect}}^{1/2}$ in bulk thermionic emitters¹⁸, in the nanoscale curved surface of a CNT. Therefore, a modified formula $I_{\text{collect}} = I_{\text{collect}}^0 \exp(\beta V_{\text{collect}})$ for the Schottky effect was adopted to describe the accelerating field regime of the $I_{\text{collect}}-V_{\text{collect}}$ plots, with I_{collect}^0 being the emission current corresponding to zero collecting voltage and β being a fitting parameter.

Emission current corresponding to zero collecting voltage (I_{collect}^0) of the CNT shown in Fig. 2a was obtained by extrapolating the accelerating field regime of its $I_{\text{collect}}-V_{\text{collect}}$ plots with the above modified formula and is shown in Fig. 2c. It can be seen that, I_{collect}^0 increases for nearly two orders from 24.9 pA to 1.9 nA, corresponding to an emission density from 82 to 6245 A m⁻², when V_{bias} increases only for 0.34 V from 2.87 to 3.21 V. Emission current density (J) was calculated from I_{collect} through $J = I_{\text{collect}}/\pi dl$ with l being the length and d being the diameter of the CNTs measured from TEM observation. We also directly measured an $I_{\text{collect}}-V_{\text{bias}}$ plot when V_{collect} was set to be 15 V (Fig. 2c). For each V_{bias} , J at $V_{\text{collect}} = 15$ V is about several times larger than that at $V_{\text{collect}} = 0$ V, which is attributed to the lowering of surface barrier due to the Schottky effect¹⁸. Figure 2c shows that I_{collect} or J increases approximately exponentially with V_{bias} for both $V_{\text{collect}} = 0$ and 15 V.

To probe the validity of Richardson's law, in addition to the measurement of electron emission density, the temperature of a CNT during electron emission should be accurately determined as well. We determined the temperature of a CNT during electron emission by measuring its thermal emission spectra. When we measured $I_{\text{collect}}-V_{\text{collect}}$ plot at a V_{bias} , the thermal emission spectrum corresponding to the bias voltage was simultaneously recorded. Figure 3a shows the thermal emission spectra of the same CNT as that shown in Fig. 2 when V_{bias} increases from 2.93 to 3.21 V at intervals of 0.04 V. The thermal emission spectra were carefully calibrated by taking into account the quantum efficiency of the optical detector and the transmission coefficient of the optical fiber (see Supplementary Fig. S2 online). Featureless blackbody emission was observed in the wavelength range of 350–750 nm, in good agreement with thermal emission spectra recorded from multiwalled CNT bundles¹⁹. It can be seen that spectrum intensity increases with V_{bias} and a blue shift is observed as V_{bias} increases, indicating the increase of CNT temperature with V_{bias} .

Fitting thermal emission spectra of individual CNTs with Planck's law has been demonstrated to be a reliable method for obtaining CNT temperature²⁰. According to Planck's law, we have

$$I(\lambda) = \frac{C}{\lambda^5} \frac{1}{\exp\left(\frac{hc}{\lambda k_B T}\right) - 1}, \quad (1)$$

where I is spectrum intensity, C is a constant, λ is wavelength, h is Planck constant, c is the speed of light in vacuum, k_B is Boltzmann constant and T is temperature. It can be seen from Fig. 3a that, our measured thermal emission spectra from individual multiwalled CNTs can be well described by Planck's law. By fitting thermal emission spectra with equation (1) (solid lines in Fig. 3a), the temperature of the CNT at each V_{bias} was obtained. Figure 3b shows the obtained temperature of the CNT in Fig. 2a at different V_{bias} . The temperature increases from 1622 to 2264 K when V_{bias} increases from 2.70 to 3.21 V. The slope of $T-V_{\text{bias}}$ plot slightly decreases at high bias voltage, indicating CNT temperature increases slightly slower with V_{bias} there. The increase of the CNT temperature is found to follow the increase of Joule-heating power ($P = I_{\text{bias}} V_{\text{bias}}$) very well (Fig. 3b).

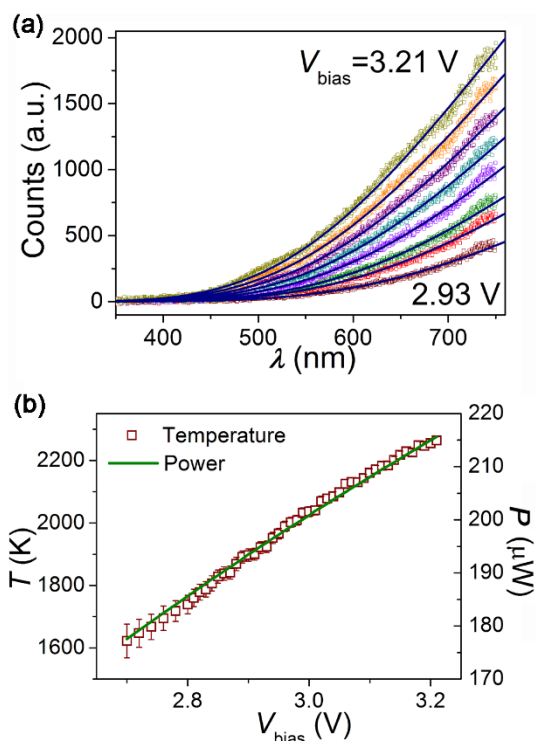


Figure 3 | Thermal emission spectra and temperature of a CNT.

(a) Thermal emission spectra of the same CNT as that shown in Fig. 2a with V_{bias} ranging from 2.93 to 3.21 V at 0.04 V intervals. The solid lines are the fitting of experimental spectra according to Planck's law. (b) $T-V_{\text{bias}}$ and $P-V_{\text{bias}}$ plots of the CNT.

After obtaining the dependences of both J and T on V_{bias} of the same CNT (Fig. 2c and 3b), we could immediately get the dependence of J on T after correlating J to T corresponding to the same V_{bias} . Figure 4a shows the $J-T$ plots of the CNT as shown in Fig. 2a. It can be seen that emission density increases approximately exponentially with temperature for both $V_{\text{collect}} = 0$ V and 15 V. When T increases for about 500 K from 1739 to 2255 K, J increases for about three orders from 57 to 2.1×10^4 A m⁻² when $V_{\text{collect}} = 15$ V. The successful determination of the dependence of emission density of a CNT on its temperature enables us to probe the validity of Richardson's law at the nanoscale.

Discussion

Richardson's law, which was firstly proposed by O. W. Richardson based on thermodynamics arguments in 1911²¹ and later by R. H. Fowler based on the quantum theory of statistics in 1928¹, is a classical law for describing thermionic electron emission from Joule-heated macroscopic metallic filaments. According to Richardson's law, thermionic emission density (J) of a hot filament is determined by its temperature and work function (W) through the following formula

$$J = AT^2 \exp\left(-\frac{W}{k_B T}\right), \quad (2)$$

where $A = (1 - r)A_0$ with r being the reflection coefficient of electrons incident on emission surface and A_0 being a constant with the value of 120.2 A cm⁻² K⁻². Since $r \ll 1$ is expected²², we have $A \sim A_0$. The formula can be rewritten as $\ln(J/T^2) = \ln A - \frac{W}{k_B T}$. The plot of $\ln(J/T^2) - 1/T$ is named as Richardson plot, which is a straight line with a constant intercept and a slope solely determined by the work function of a filament. To compare our measured electron emission from individual CNTs with Richardson's law, the data shown in

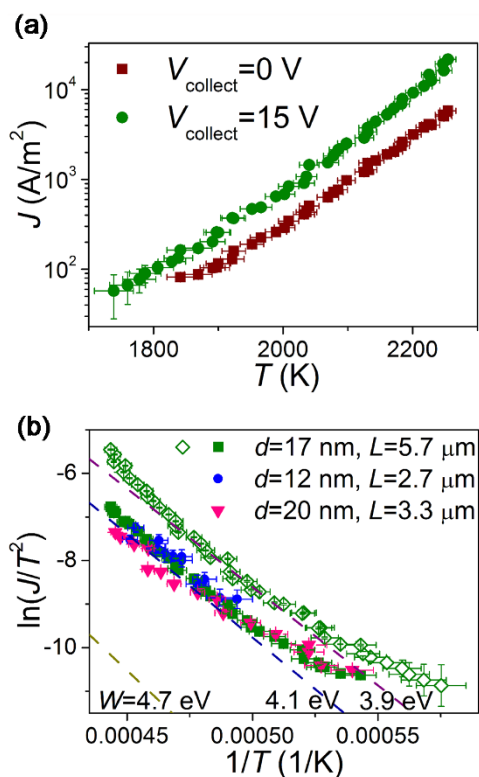


Figure 4 | Comparison of experimental data with Richardson's law.

(a) J - T plots of the same CNT as that shown in Fig. 2a with $V_{\text{collect}} = 0$ and 15 V. (b) $\ln(J/T^2) - 1/T$ plots of three CNTs with J in the unit of A m^{-2} and T in the unit of K. Solid symbols correspond to $V_{\text{collect}} = 0$ V while hollow symbols correspond to $V_{\text{collect}} = 15$ V. The length and diameter of CNTs are shown in (b). The dashed lines are Richardson plots with $W = 3.9, 4.1$ and 4.7 eV.

Fig. 4a was replotted in the form of $\ln(J/T^2)$ versus $1/T$ (Fig. 4b), together with the experimental data corresponding to $V_{\text{collect}} = 0$ V of another two CNTs. The experimental data corresponding to $V_{\text{collect}} = 15$ V of the three CNTs is shown in Supplementary Fig. S3 online. It can be seen from Fig. 4b and S3 that measurement results from different CNTs coincide very well, implying good replicability of our measurements.

Interestingly, experimental $\ln(J/T^2) - 1/T$ plots of individual CNTs are found to exhibit an upward bending feature (Fig. 4b), obviously deviating from the straight lines in Richardson plots. The experimental plots corresponding to $V_{\text{collect}} = 0$ V coincides well with the Richardson plot of $W = 4.1$ eV at high temperature range, but starts to bend upward and deviates from the Richardson plot at lower temperature range. The deviation from Richardson plot is also verified by the experimental plot corresponding to $V_{\text{collect}} = 15$ V. It coincides with the Richardson plot of $W = 3.9$ eV at mediate temperature range but starts to bend upward at both high and low temperature range.

In addition to the upward bending feature in the experimental $\ln(J/T^2) - 1/T$ plots, our measured emission density is found to be much higher than that predicted by Richardson's law. The work function of the side surface of CNTs was measured to be 4.7 – 4.9 eV¹¹. If we assume a work function of 4.7 eV for CNT side surface, our measured emission density is more than one order of magnitude higher than that predicted by Richardson's law and the difference between experimental data and theoretical prediction becomes more and more significant as temperature decreases due to the upward bending feature (Fig. 4b). Considering that macroscopic graphite has a similar work function as that of CNTs^{23,24}, our results imply that individual CNTs exhibit much better electron

emission performance as compared to its macroscopic allotrope, of which thermionic emission is assumed to follow Richardson's law.

As shown in Fig. 2, our studied CNTs were heated by self-Joule heating and suspended between two relatively large metal probes that act as heat sinks. CNTs heated by such a setup are expected to have a non-uniform temperature profile²⁵, which may maximize in the middle of a tube, and thus a non-uniform emission density distribution along the tube axis. Since the tube section with a higher temperature induces a stronger thermal light emission, our collected thermal light emission was mainly from the hottest tube section in the middle. So our determined temperature can be considered as the peak temperature along a CNT, while the determined emission density is the averaged density of the whole tube. If we consider electron emission from the tube section exhibiting a temperature as we determined, then its emission density is underestimated here. Therefore, the actual deviation of the electron emission from self-Joule-heated CNTs from Richardson's law is expected to be more significant than that shown in Fig. 4b.

Five CNTs were studied in our experiments in total (see Supplementary Fig. S3 for the results of another two CNTs). The electron emission performances of all the five CNTs deviate from Richardson's law in the same manner. Therefore, we conclude that Richardson's law fails to describe electron emission from individual self-Joule-heated CNTs. The breakdown of Richardson's law can be attributed to the following reasons. First, Richardson's law is based on a 3D atmosphere of free electrons in metals¹, but quasi-one-dimensional (quasi-1D) CNTs obviously deviate from 3D free electron systems. Second, while Richardson's law was derived by applying the Fermi-Dirac statistics to a 3D free electron atmosphere¹, the distribution of electrons in an electrically-biased CNT was found to deviate much from Fermi-Dirac distribution, especially at high energy states close to the vacuum level, due to quasi-1D character of CNTs and their special characteristics of electron-phonon coupling²⁶. The significant effect of bias voltage (or internal electric field) on the distribution of electrons in a CNT makes internal electric field along a CNT, together with thermal effect, co-contribute to electron emission from it¹⁷. Third, nanoscale thickness of our studied CNTs makes their electrons be confined in a 10 – 20 nm wide cylindrical quantum well formed by surface energy barrier along emission direction. Such quantum confinement is absent in macroscopic thermionic emitters and may also make our measured electron emission deviate from Richardson's law.

Our conclusion on the validity of Richardson's law in the electron emission from self-Joule-heated CNTs is in contrary to that in a previous report, where electron emission from self-Joule-heated CNT yarns was found to follow the straight Richardson plot with $W \sim 4.6$ eV and $A \sim 120$ $\text{A cm}^{-2} \text{K}^{-2}$ very well in a temperature range similar to that in our measurements¹⁰. The contrary conclusions are thought to be caused by the different dimensions of the samples studied in the report and our experiments. While individual CNTs with a diameter of 10 – 20 nm and a length of several microns were studied in our experiments, 20 μm thick and 8 mm long CNT yarns consisting of a large number of individual CNTs were studied in the report. Such a large size of the CNT yarns is believed to degrade the above discussed characters of CNTs responsible for the breakdown of Richardson's law, and makes CNT yarns behave like macroscopic metallic filaments and follow Richardson's law well. Therefore, electron emission performance of individual CNTs, of which emission current is more than one order of magnitude higher than that predicted by Richardson's law as shown above, is seriously degraded in forming CNT yarns.

The breakdown of Richardson's law at the nanoscale implies an urgent need of developing new theoretical descriptions of electron emission from individual low-dimensional nanostructures, where all characters associated with the nanoscale size and low dimensionality of nanostructures, e.g. low-dimensional electron atmosphere,



non-equilibrium electron distribution, quantum well confinement, modified image potential, *etc.*, should be well taken into account²⁷. Those characters peculiar to low-dimensional nanostructures are expected to induce new properties of electron emission and potential applications.

In summary, we report on experimental evidence that electron emission density (J) from individual self-Joule-heated CNTs at different temperature (T) does not obey classical Richardson's law of thermionic emission. Experimental $\ln(J/T^2) - 1/T$ plots exhibit an upward bending feature deviating much from the straight lines in Richardson plots and the measured electron emission density is more than one order of magnitude higher than that predicted by Richardson's law. The breakdown of Richardson's law implies much better electron emission performance of individual CNTs as compared to their macroscopic allotropes and clusters, and an urgent need of new theoretical descriptions of electron emission from individual low-dimensional nanostructures.

Methods

Our experiments were performed *in situ* in a FEI Quanta 600F scanning electron microscope (SEM) with four Kleindiek MM3A nanomanipulators installed in the SEM chamber. The vacuum level in SEM chamber was $\sim 5 \times 10^{-4}$ Pa. Three of the nanomanipulators were each equipped with a 100–500 nm wide W tip working as an electrical probe and the fourth one was equipped with an 10–30 μm wide optical fiber tip working as an optical probe. Both W tips and optical fiber tip were made by chemically etching and a 40 nm Pd or 10 nm Ag film was coated on the optical fiber tip to avoid electric charging under electron beam irradiation. Under the control of nanomanipulators, each probe can move in three directions with a step size as small as a few nanometers. The three electrical probes were connected to a Keithley 4200 semiconductor characterizing system for electrical measurements and the optical probe was connected to a Horiba Jobin Yvon iHR320 spectrometer equipped with a Synapse CCD detector for optical spectrum recording. Electron beam of SEM was blanked during the measurements, so the effects of electron beam irradiation on the measurements are absent.

Arc-discharge grown multiwalled CNTs were used in our experiments²⁸. They were introduced into SEM chamber through a Pt wire, which was dipped into the carbon deposit grown on the negative carbon electrode of arc-discharge to make some CNTs attached to it. To obtain a CNT for measurements, an individual CNT protruding from the edge of the Pt wire was firstly connected by a W tip (see Supplementary Fig. S4 online), then it was separated from the Pt wire by applying a gradually increasing voltage between the Pt wire and W tip until it broke down. After a CNT adhered to a W tip was obtained, it was manipulated to make contact with the second W tip. The third W tip and an optical fiber tip were then manipulated to approach the CNT to set up the multi-probe measurement configuration as shown in Fig. 1a. TEM images indicate that CNTs used in our experiments have uniform diameter and very good tubular structure without visible defects (see Supplementary Fig. S4). Their near-perfect structure ensures that our measured electron emission was from a homogeneous surface of honeycomb carbon lattice. After measurements in SEM were completed, CNTs were placed onto the carbon film of a TEM grid and were then transferred into a TEM (FEI Tecnai G20) for structure characterization (see Supplementary Fig. S5 online). TEM images indicate that the tubular structure of a CNT was well preserved after measurements (inset of Fig. 2a and Supplementary Fig. S5).

The extrapolation of the accelerating field regime of $I_{\text{collect}} - V_{\text{collect}}$ plots and the fitting of thermal emission spectra with the Planck's law were performed by using the non-linear least-square fitting function of MATLAB software (*lsqcurvefit*), with I_{collect}^0 and β , T and C as fitting parameters, respectively. The error of the fitting parameter was evaluated through $\sigma_i = \sqrt{C_{ii}\chi^2}$, where χ^2 is the squared 2-norm of the residual of least-square fitting, C_{ii} is the diagonal elements of the matrix $C = (F^T \times F)^{-1}$ with F being the Jacobian matrix of the fitting function.

1. Fowler, R. H. The restored electron theory of metals and thermionic formulae. *Proc. R. Soc. Lond. A* **117**, 549–552 (1928).
2. Fowler, R. H. & Nordheim, L. Electron emission in intense electric fields. *Proc. R. Soc. Lond. A* **119**, 173–181 (1928).
3. Cox, D. C., Forrest, R. D., Smith, P. R. & Silva, S. R. P. Thermionic emission from defective carbon nanotubes. *Appl. Phys. Lett.* **85**, 2065–2067 (2004).
4. Liu, P. *et al.* Thermionic emission and work function of multiwalled carbon nanotube yarns. *Phys. Rev. B* **73**, 235412 (2006).
5. de Jonge, N., Lamy, Y., Schoots, K. & Oosterkamp, T. H. High brightness electron beam from a multi-walled carbon nanotube. *Nature* **420**, 393–395 (2002).
6. Wang, M. S., Wang, J. Y. & Peng, L. M. Engineering the cap structure of individual carbon nanotubes and corresponding electron field emission characteristics. *Appl. Phys. Lett.* **88**, 243108 (2006).
7. Bonard, J.-M., Dean, K. A., Coll, B. F. & Klinke, C. Field emission of individual carbon nanotubes in the scanning electron microscope. *Phys. Rev. Lett.* **89**, 197602 (2002).

8. Wu, Z.-S. *et al.* Field emission of single-layer graphene films prepared by electrophoretic deposition. *Adv. Mater.* **21**, 1756–1760 (2009).
9. Xiao, Z. M. *et al.* Field electron emission characteristics and physical mechanism of individual single-layer graphene. *ACS Nano* **4**, 6332–6336 (2010).
10. Wei, Y. *et al.* Comparative studies of multiwalled carbon nanotube sheets before and after shrinking. *Phys. Rev. B* **76**, 045423 (2007).
11. Liu, P. *et al.* Measuring the work function of carbon nanotubes with thermionic method. *Nano Lett.* **8**, 647–651 (2008).
12. Wu, J. F., Wyse, M., McClain, D., Thomas, D. & Jiao, J. Fabrication and field emission properties of triode-type carbon nanotube emitter arrays. *Nano Lett.* **9**, 595–600 (2009).
13. Wang, M. S., Chen, Q. & Peng, L. M. Field-emission characteristics of individual carbon nanotubes with a conical tip: the validity of the Fowler–Nordheim theory and maximum emission current. *Small* **4**, 1907–1912 (2008).
14. Collins, P. G. & Zettl, A. Unique characteristics of cold cathode carbon-nanotube-matrix field emitters. *Phys. Rev. B* **55**, 9391–9399 (1997).
15. Wei, X. L., Chen, Q., Peng, L. M., Cui, R. L. & Li, Y. *In situ* measurements on individual thin carbon nanotubes using nanomanipulators inside a scanning electron microscope. *Ultramicroscopy* **110**, 182–189 (2010).
16. Bournon, B. *et al.* Geometrical dependence of high-bias current in multiwalled carbon nanotubes. *Phys. Rev. Lett.* **92**, 026804 (2004).
17. Wei, X. L., Golberg, D., Chen, Q., Bando, Y. & Peng, L.-M. Electric-field-direction dependent spatial distribution of electron emission along electrically biased carbon nanotubes. *Phys. Rev. B* **84**, 195462 (2011).
18. Herring, C. & Nichols, M. H. Thermionic emission. *Rev. Mod. Phys.* **21**, 185–270 (1949).
19. Li, P. *et al.* Polarized incandescent light emission from carbon nanotubes. *Appl. Phys. Lett.* **82**, 1763–1765 (2003).
20. Liu, Z. W., Bushmaker, A., Aykol, M. & Cronin, S. B. Thermal emission spectra from individual suspended carbon nanotubes. *ACS Nano* **5**, 4634–4640 (2011).
21. Richardson, O. W. Electron emission from metals as a function of temperature. *Phys. Rev.* **23**, 153–155 (1924).
22. Nordheim, L. W. The effect of the image force on the emission and reflexion of electrons by metals. *Proc. R. Soc. Lond. A* **121**, 626–639 (1928).
23. Shiraishi, M. & Ata, M. Work function of carbon nanotubes. *Carbon* **39**, 1913–1917 (2001).
24. Su, W. S., Leung, T. C. & Chan, C. T. Work function of single-walled and multiwalled carbon nanotubes: First-principles study. *Phys. Rev. B* **76**, 235413 (2007).
25. Wei, X. L., Liu, Y., Chen, Q. & Peng, L. M. Controlling electron beam induced carbon deposition on carbon nanotubes by joule heating. *Nanotechnology* **19**, 355304 (2008).
26. Wei, X. L., Golberg, D., Chen, Q., Bando, Y. & Peng, L. M. Phonon-assisted electron emission from individual carbon nanotubes. *Nano Lett.* **11**, 734–739 (2011).
27. Wei, X. L., Chen, Q. & Peng, L. M. Electron emission from a two-dimensional crystal with atomic thickness. *AIP Adv.* **3**, 042130 (2013).
28. Ando, Y. & Iijima, S. Preparation of carbon nanotubes by arc-discharge evaporation. *Jpn. J. Appl. Phys.* **32**, L107–L109 (1993).

Acknowledgments

This work was supported by the National Basic Research Program of China (Grant No. 2013CB933604), National Natural Science Foundation of China (Grant No. 61371001, 61321001 and 11304003), and the Foundation for the Author of National Excellent Doctoral Dissertation of China (Grant No. 201241) and Specialized Research Fund for the Doctoral Program of Higher Education of China (Grant No. 20130001110030). X.W. thanks Dr. C. L. and Dr. C. Z. for valuable discussions.

Author contributions

X.W. designed and performed the experiments, analyzed the data, and wrote the paper. S.W., Q.C. and L.P. contributed significant discussions and suggestions, and commented on the manuscript.

Additional information

Supplementary information accompanies this paper at <http://www.nature.com/scientificreports>

Competing financial interests: The authors declare no competing financial interests.

How to cite this article: Wei, X., Wang, S., Chen, Q. & Peng, L. Breakdown of Richardson's Law in Electron Emission from Individual Self-Joule-Heated Carbon Nanotubes. *Sci. Rep.* **4**, 5102; DOI:10.1038/srep05102 (2014).



This work is licensed under a Creative Commons Attribution-NonCommercial-NoDerivs 3.0 Unported License. The images in this article are included in the article's Creative Commons license, unless indicated otherwise in the image credit; if the image is not included under the Creative Commons license, users will need to obtain permission from the license holder in order to reproduce the image. To view a copy of this license, visit <http://creativecommons.org/licenses/by-nc-nd/3.0/>